ASSOCIATED CONTENT

Supporting Information

Lithium-ion battery (LIB) immersed in fire prevention material for fire safety and heat management

Material – Composition and Construction of the BIF

FPM Synthesis. The polyvinyl alcohol (PVA) powder is added to distilled water and stirred to prepare the first solution, the 15 wt% PVA. The heating mantle is additionally used for better dissolution of PVA powder into water. The boric acid powder is added to distilled water to produce the 1 wt% boric acid solution. By mixing and stirring the first solution, the second solution, distilled water, $NaHCO_3$, and fumed silica powder, the fire extinguishing agent used for BIF is synthesized.

Sealing. Firstly, the multilayer film sealing composed of polyurethane, polyacrylate, ABS resin, and polyvinyl chloride is applied to the cell bodies. Secondly, the Epoxy is mixed with polyamide and polyamine to protect cell tabs from the FPM.

BIF Module Assembly. For the construction of the battery module, the batteries are fastened with the cell holder and Ni-tab was spotted for the construction of the module. Then, the epoxy sealing was poured on the cell tabs. Finally, the batteries are inserted into the case and immersed with the FPM.

Experimental – Supplementary Experiments of FPM

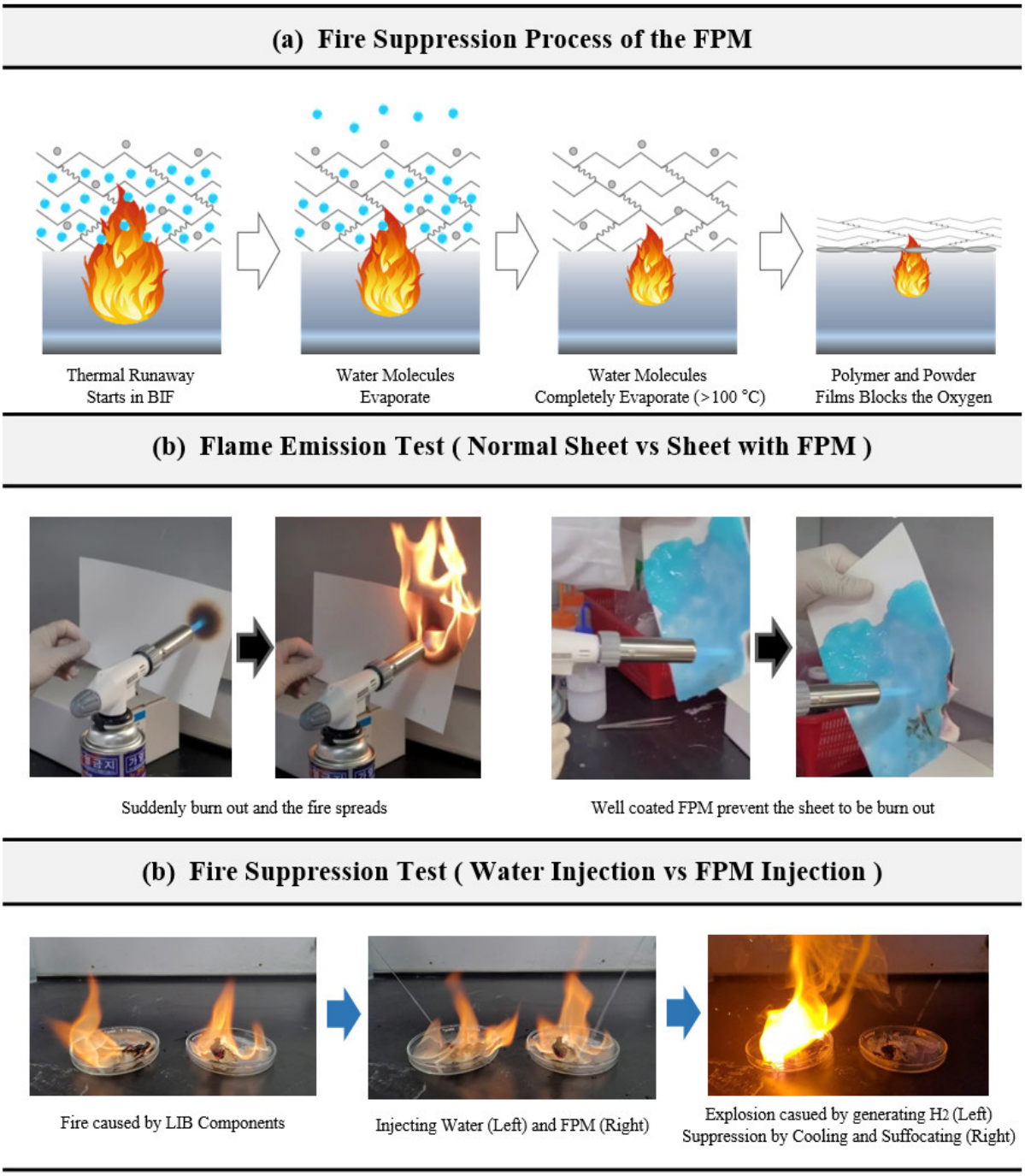

Figure S1 (a) Fire Suppression Process of the FPM when thermal runaway happens in battery
(b) Flame emission Test on a normal paper sheet and the sheet with the FPM
(c) Fire suppression test by injection of water and the FPM

Fire Suppression Process. Figure S1 (a) shows the fire suppression process of the FPM. Due to the immersion, the FPM always surrounds the surface of the battery cell. When thermal runaway occurs, the water molecules, located close to the fire, are evaporated by the heat of the fire. The water molecules remaining in the polymer move toward the polymer chain covering the upper part of the battery to prevent the polymer from being burned by cooling. As the water evaporates, the polymer chain near the fire covers the surface of the battery to block the contact of oxygen. After that, when the water in the polymer is all evaporated, the polymer and expanded glass are coated on the battery surface.

Flame Emission Test. In Figure S1 (b), The flame was emitted by the torch (~750 °C) to the normal paper sheet and the FPM-coated sheet to verify the cooling effect of the FPM. The fire immediately occurs when a fire is emitted on a normal paper. The shape of the paper is deformed, a black scorch with ash is generated, and the fire spreads to the surrounding area. By coating or applying the FPM to the sheet, it can be confirmed that the fire does not occur well. Also, the fire does not spread to the surrounding area, and the combustion reaction rate is significantly reduced.

Fire Suppression Test. In Figure S1 (c), the battery fire situation was simulated by firing the mixture of an electrolyte (1.2M LiPF6 in DEGDME 3mL), a separator (0.1g PP separator), and a metal (Li Metal 0.12g). Thereafter, the distilled water and FPM were sprayed respectively to confirm the fire suppression performance. After the generation of the fire, 5 mL of general distilled water (left sample) of was sprayed and 5 mL of FPM (right sample) was sprayed each. In the case of spraying distilled water, the fire occurred more significantly due to the production of the hydrogen and the oxygen supply from the air. In the case of spraying the FPM, the fire was immediately extinguished, and it was confirmed that a coating film was formed on the surface of the battery.

Material – Comparison of Battery Fre Suppression Agent Properties

	Halon 1211	HFC -227ea (FM-200)	NOVEC 1230	ABC (NH_4 H_2PO_4)	F-500 + Water (mist)	FPM	K-type (KNO_3 Based)	S-type ($Sr(NO_{32}$ Based)
Extinguish Method	Inhibition of radical reaction	Suffocate, Inhibition of radical reaction	Cooling, Inhibition of radical reaction	Suffocate, Inhibition of radical reaction	Cooling, Inhibition of radical reaction	Cooling, Suffocate	Suffocate, Inhibition of radical reaction	
Phase	Gas	Gas	Liquid	Solid	Liquid	Liquid	Solid, Gas	
Heat Capacity (J/g·K)	0.4493	0.81327	1.103	1.19	-	**3.925**	-	
Latent Heat (J/g)	-	-	88.0	-	-	**2,125**	-	
Heat Conductivity (W/m·K)	-	0.013336	0.059	-	-	**0.559**	-	
Electrical Conductivity (mS/cm)	Non-conductive	Non-conductive	Non-conductive	Non-conductive	-	**3.456**	Non-conductive	
Dielectric Constant	-	2	2.3	12	-	**-**	-	

Table S1 Material properties comparison table for the agent used for battery fire

FPM Property. Table S1 (a) compares the material properties of the agents used for battery fire suppression. Compared to other agents, FPM shows superior high heat capacity, latent heat, and heat conductivity. The advantages are as follows. First, high heat conductivity enables FPM to promptly absorb the heat generation from the battery and dissipate it. Second, high heat capacity prevents the temperature increment of FPM even though it absorbs lots of heat. Lastly, the high latent energy enables to removal of the heat from the battery when thermal runaways happen.

However, electrical conductivity is crucial for battery corrosion and short circuits. So specialized sealing layers are adopted to the battery cell in this study.

Experiment Condition – Computational Solver with Methods and Conditions

Computational Solver. The battery simulation was performed using the Multi-scale Multi-Domain (MSMD) model in the computational fluid dynamics (CFD) program Ansys Fluent, which combines electrochemical reaction, heat transfer, and fluid flow calculations. Specifically, a 2RC equivalent circuit model (ECM) was used, which simulates the electrical behavior of the cell by mimicking an electrical circuit as a detailed model of the electrochemical reaction. The model was used as a detailed model of the electrochemical reaction. It consists of six parameters: one open voltage, two capacitors, and three resistors, and the values of each parameter were extracted using the hybrid pulse power characterization (HPPC) test.

Mesh. Mesh is composed of 18650 single cell and module with tetrahedral geometry. Mesh software ANSYS Fluent with adaptive sizing was used, and mesh independence checks were performed by increasing the number of elements and comparing the cell temperature results at discharge. After adding 54,937 elements to the single cell and 349,362 elements to the module, the cell temperature converged to within 0.1°C. The quality of the constructed mesh was enough to achieve uniform simulation results, so we used this mesh to perform the simulation.

Boundary Condition.

- $Q_{dissipation} = Q_{convection} + Q_{radiation}$
- $Q_{convection} = hA_{bat.sys}(T_{bat.sys} - T_{ambient})$
- $Q_{radiation} = \sigma\varepsilon_{bat.sys}A_{bat.sys}(T_{bat.sys}^4 - T_{ambient}^4)$

(h : natural convection heat transfer coefficient, $A_{bat.sys}$: the battery surface area, $T_{bat.sys}$: the battery surface temperature, $T_{ambient}$: the ambient temperature, σ : Stefan-Boltzmann constant, $\varepsilon_{bat.sys}$: emissivity of the outside of the battery.)

Free convection	Heat transfer coefficient [$W/m^2 \cdot K$]	5
	Free stream temperature [°C]	25
Radiation	Stefan-Boltzmann constant [$W/m^2 \cdot K^4$]	$5.6704 * 10^{-8}$
	External emissivity [-]	0.8
	External radiation temperature [°C]	25

Model. The multiphase cell and module used for the CFD are explained in Figure 3 in the manuscript.

Experimental – Thermal Runaway Test of the LIB and BIF Cell

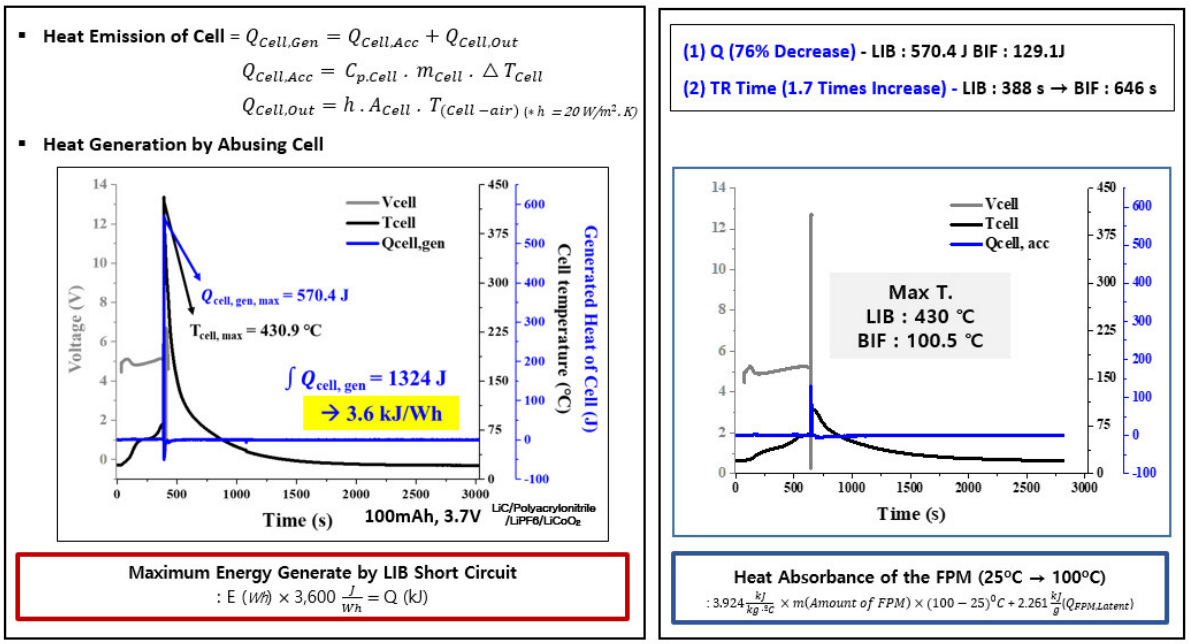

Figure S2 Maximum energy generated by LIB short circuit, and the heat absorbance performance of BIF when theoretical amount of the FPM is applied to the cell (3.7 V / 50 mAh / LCO Pouch cell)

Figure S2 shows the result of the thermal runaway test of LIB and BIF to verify the cooling effect of the FPM when the theoretical amount is applied. The cell (3.7 V / 50 mAh / LCO Pouch type) was overcharged and the voltage, temperature, and generation of the heat were measured. The maximum heat generation amount(570.4 J) was the same as the theoretical amount from the reference in Equation (1) in the manuscript. When a theretical amount of the FPM is applied to the BIF in the same condition, the heat generation of the cell was decreased by about 76 %, the 129.1 J. Also, the maximum temperature of the cell was decreased from 430 °C to 100.5 °C. and the fire was not observed. Additionally, due to the cooling effect of the FPM in BIF, the time to lead the thermal runaway was postponed from 388 seconds to 646 seconds.

Principle – Chain Reactions of Lithium-ion Battery by Thermal Runaway Stages with Temperatures

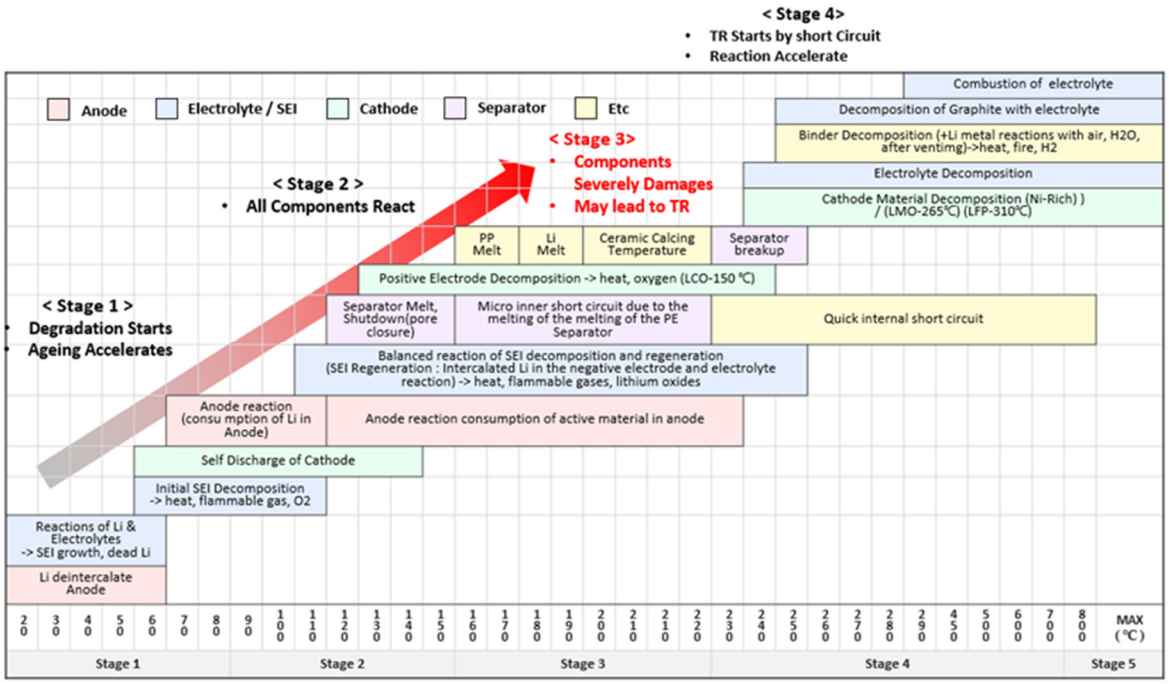

Figure S3. Exothermic chain reactions of LIB by thermal runaway stages

Figure S3 shows the stages of thermal runaway of the LIB by temperature and its constituent materials, referring to previous studies [58,66,77,87]. The reactions by stage and temperature were obtained from previous research [58,66,77]. The temperature control of BIF relieves battery aging during operation at stage 1 and prevents it from reaching stage 2 by thermal management. Although thermal runaway occurs at stages 3 and 4, direct FPM penetration into the cell in the BIF is suppressed to satisfy the requirements for fire conditions and propagation. Even though the thermal runaway happens in stage 4, the thermal runaway reaction starts at 20°C and it is a chain reaction. So lowering the temperature affects the safe operation of the battery. The description of the thermal runaway stages is as follows.

Stage 1 relates to the battery operating condition (under 90 °C), that is, the temperature range that the battery can easily reach during the battery cycle under harsh conditions. At this temperature, the battery suffers from aging and degradation, which affect its electrochemical performance. In addition, reactions such as the initial SEI decomposition, self-discharge of the cathode, and anode reactions start [31,32,53]. In the early stages of stage 2, all materials in the battery suffer severe damage caused by heat generation. The materials composing the battery melt, and reactions such as the consumption or regeneration of the material occur. Moreover, the battery was designed and constructed to stop operation at these temperatures through protection devices in both internal devices inside the battery, such as the

positive temperature coefficient (PTC) and current interrupt device (CID), and outer devices, such as the BMS [18]. In stage 3, the pressure increases owing to gas evolution and the internal short circuit caused by melting, leading to the early stages of thermal runaway. Finally, in stages 4 and 5, the reaction accelerates and finally reaches thermal runaway with combustion.

Experimental – Electrochemical Performance Comparison at Low Temperature (5 ºC) in LIB and BIF

Figure S4 shows a comparison of the capacity by cycle and voltage efficiency between the LIB and BIF at a low temperature. As shown in the graph, the surface temperature of the LIB was sufficiently high (53 ºC) to allow for adequate performance. However, the BIF sustained the low temperature, which led to large capacity decreases during long cycling. The high capacity of the FPM maintained a surface temperature of the battery equal to that of the external environment [79,88].

The discharge capacity resistance increased at a high C-rate and low temperature. Ageing of the battery accelerated as the cycle progressed. The electrolyte conductivity decrease and sluggish reaction made it difficult for discharge reactions to occur, because of an increase in the internal resistance. Decreasing the number of ions participating in the reaction finally led to a decrease in the life-cycle length. The diffusion rate decreased owing to the polarization of electrodes caused by high electrode activity based on the cell design and SEI, and the electrolytes increased the impedance, which worsened with increases in the operating current. A persistently high C-rate at a low temperature may lead to lithium plating, SEI thickening, and destruction, while diffusion may become difficult. This leads to high non-linearity in the BIF.

Moreover, a temperature below the –20 ºC, not only affects diffusion of electrolytes but also the electrodes themselves.

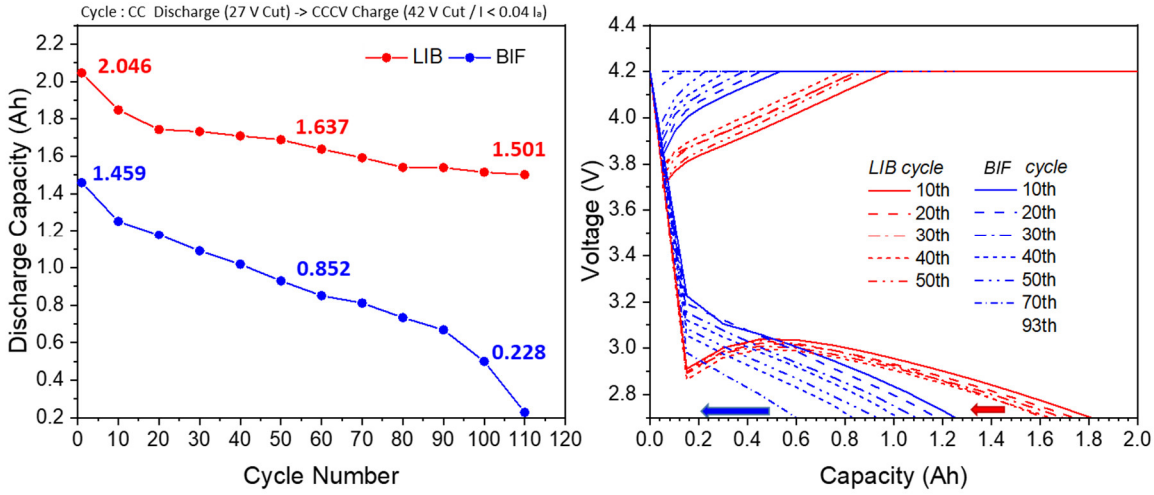

Figure S4. Capacity by cycle and voltage efficiency comparison between LIB and BIF at low temperature (5 ℃)

Experimental – Battery Degradation Mechanisms in BIF

Normally, there are numerous influencing factors that effects the performance of the battery and cause degradation [58,66,77]. In the EIS experiments shown in Figure 8, the influencing factors are a high temperature and high current. Room temperature was approximately 40 ºC, while the maximum temperatures in the LIB and BIF were 90 ºC and 63 ºC, respectively. The discharge C-rate was approximately 4, while the charge was 1.

As illustrated in Figure S5, the influencing factor, a high temperature, can lead to SEI decomposition, SEI growth, electrolyte decomposition, and binder decomposition. SEI degradation was the first process to occur sufficiently at room temperature. However, it did not occur in the NCA LIB for a short time. Electrolyte decomposition occurred during the second process of battery degradation, at temperatures above 60 ºC, in the LIB, while the binder decomposed at temperatures above 100 ºC. This resulted in bulk resistance(Rb) remaining constant.

At a high current, structural disordering and the side reactions, such as carbon exfoliation, contact loss, dendrite formation, and Li plating, occurred. Electrode particle cracking occurred due to structural disordering. However, the side reactions at the upsides did not yet occur, based on the EIS results in Figure 8 in the manuscript.

The degradation mechanisms of electrolyte decomposition and the structural disordering resulted in a loss of active material, a loss of electrolytes, and an increase in impedance. Specifically, the loss of electrolyte simultaneously affected the loss of active material and increase in impedance in the degradation mode. These effect the decrease in mass transport and eventually the capacity and power fading simultaneously. These factors likely increase the 2nd semicircle (Rct: charge-transfer resistance).

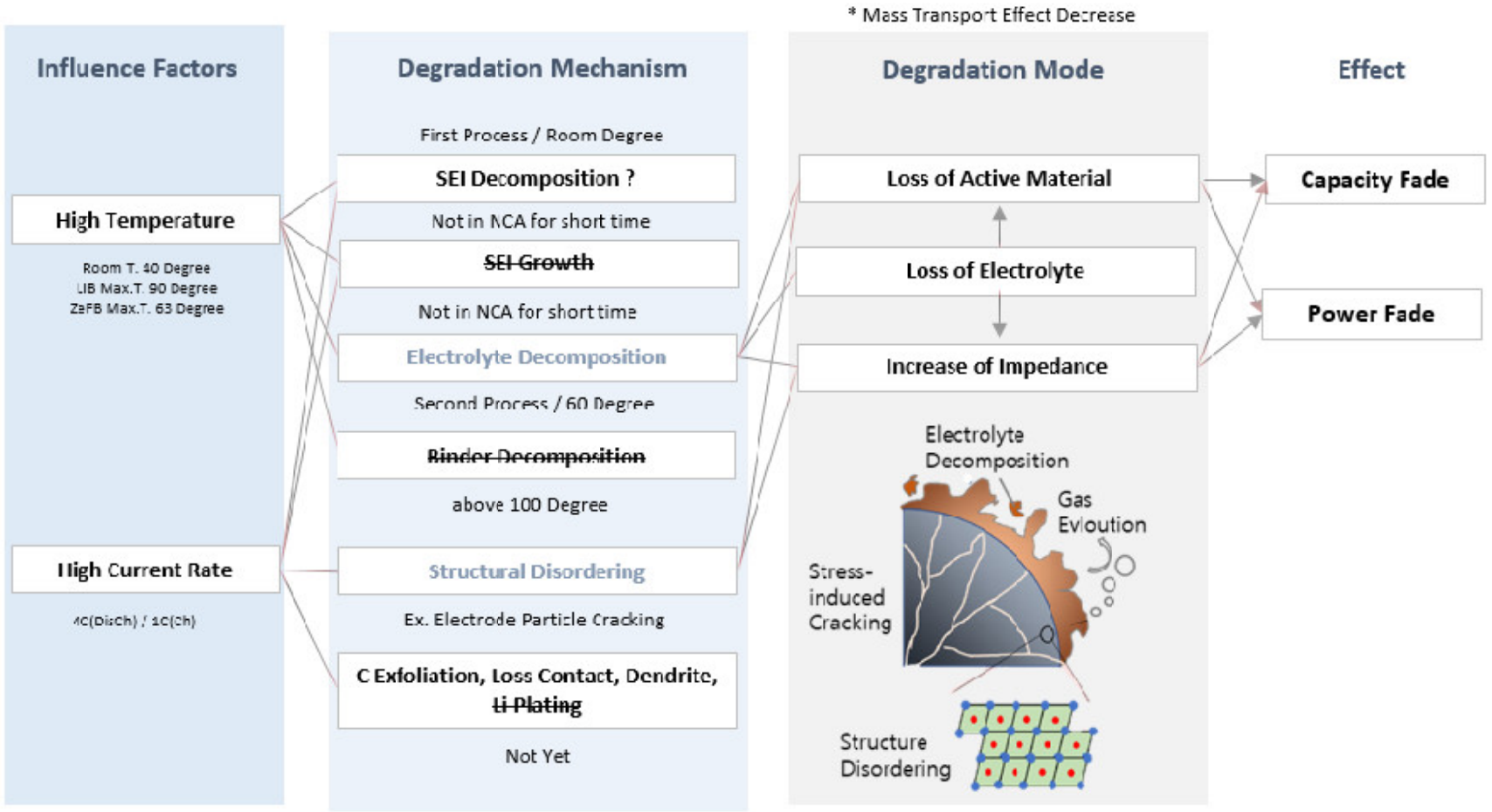

Figure S5. Influencing factors and degradation mechanisms of BIF during cycling

Experimental – △ V and Resistance with Gradual C-Rate Increase

Electrochemical performance at a high C-rate is essential for battery applications such as those in EVs. The experiments depicted in Figure 9 show the temperature and voltage efficiency of a LIB and BIF with a C-rate. The voltage difference (△V) and resistance were measured at each cycle step. The voltage differences of the LIB and BIF shown in Figure S6 were measured by ohmic discharge, non-ohmic discharge, ohmic charge, and non-ohmic charge.

During ohmic discharge, the end process of charge, the temperatures of both the LIB and BIF were almost 40 ºC. Thus, there was no temperature difference. Therefore, the voltage difference was proportional to the C-rate increase. However, non-ohmic discharge showed different results. In the BIF, the low temperature, caused by thermal management, decreased the available capacity, resulting in a drastic voltage drop with a C-rate increase. Therefore, the slope of the non-ohmic discharge of LIB is lower than that of the BIF. The ohmic charge step was the period, which is the end step of discharge and represents the highest temperature in each cycle. Similarly, resistance decreased proportionally to temperature increases. At this time, the slope of the LIB was higher than that of the BIF. Lastly, during non-ohmic charge, only the C-rate had a minor effect.

Figure S7 shows the resistance difference with the C-rate. In all the graphs, the BIF shows a higher resistance value than the LIB because of the temperature. The only exception is the ohmic discharge process, where there is no temperature gap between the LIB and BIF, and all the results are inversely proportional to the C-rate, showing a curved shape.

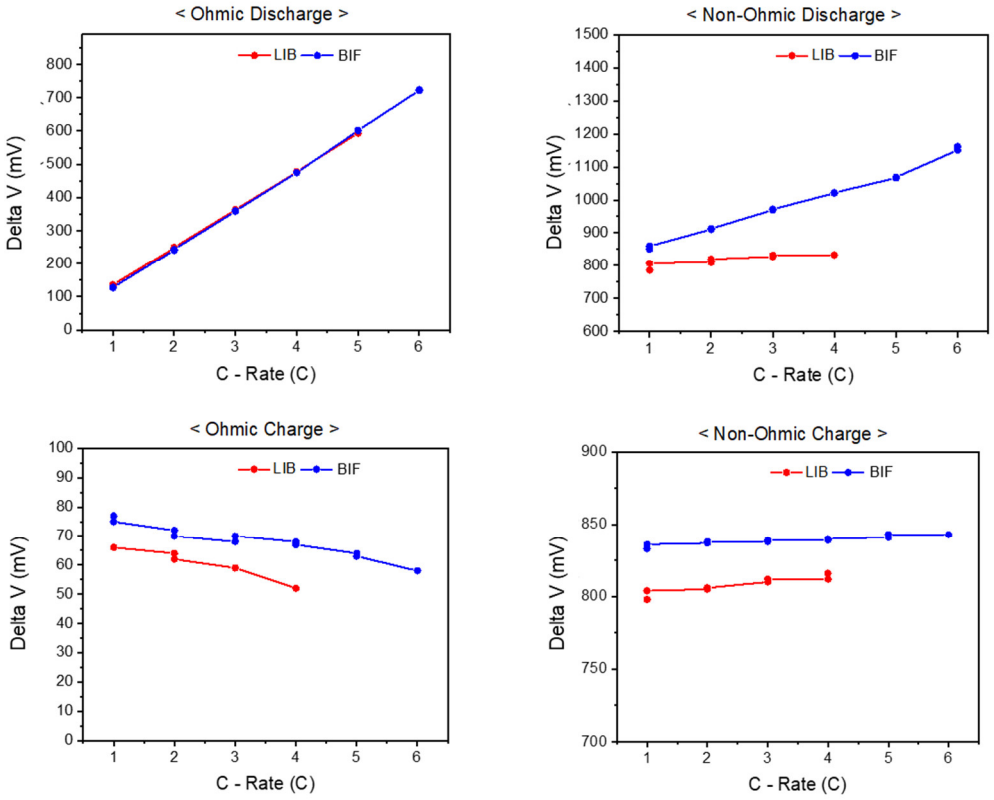

Figure S6. Delta V comparisons with gradual C-rate increases for LIB and BIF

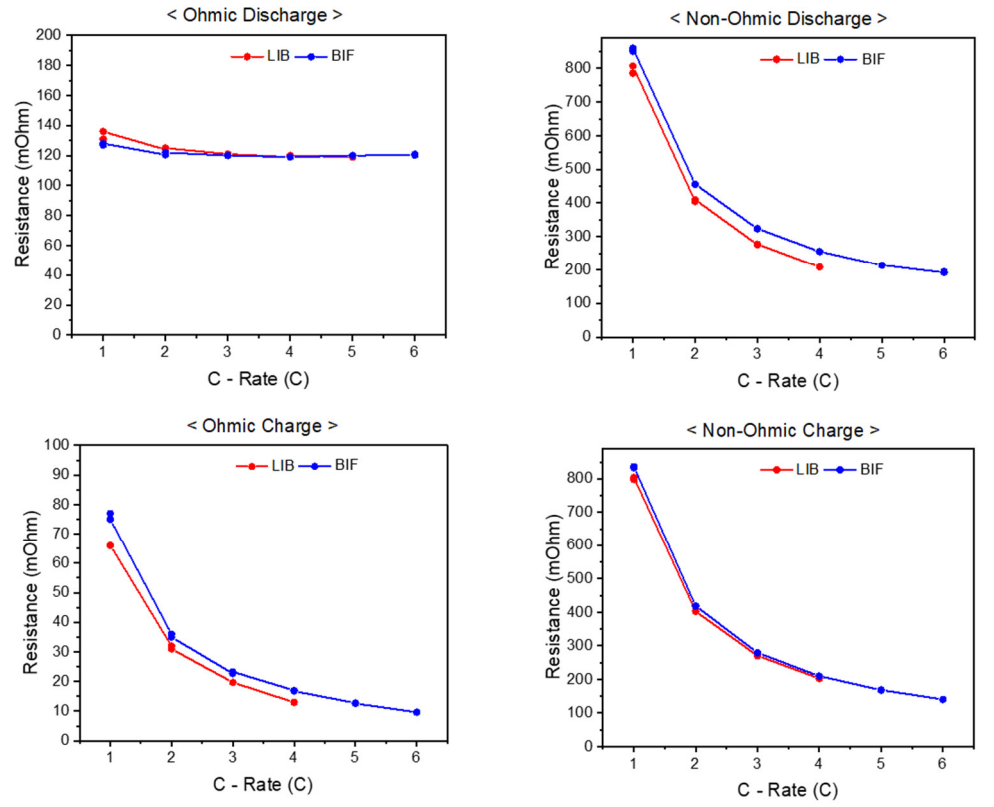

Figure S7. Resistance comparisons by gradual C-rate increases of LIB and BIF

Experimental – Temperature of the BIF Module by Spots

Unlike single cells, the temperature of the module differed by spots. Figure S8 illustrates the locations of the maximum temperature of 15 spots during the cycle. The locations were randomly distributed and include the surface of the batteries, such as the spots between two cells, and the center of four cells. Measuring the temperatures of irregular spots has the advantage of determining the temperature tendency of the entire module. The maximum-temperature spots were always the center of the module. They were 29.5 ºC in 0.2 C-rate cycling, 32.1 ºC in 0.3 C-rate cycling, and 38.4 ºC in 0.5 C-rate cycling. The chamber's room temperature was approximately maintained at 25 ºC. When the results of 0.5 C-rate data were fitted to the temperature diagram, they revealed a regular temperature distribution with high temperatures at the center and low temperatures at the sides [83].

Figure S9 illustrates the voltage, current, cell temperatures, chamber temperature, and case temperature simultaneously. The tendency and configuration of the cell temperature should be studied in more detail.

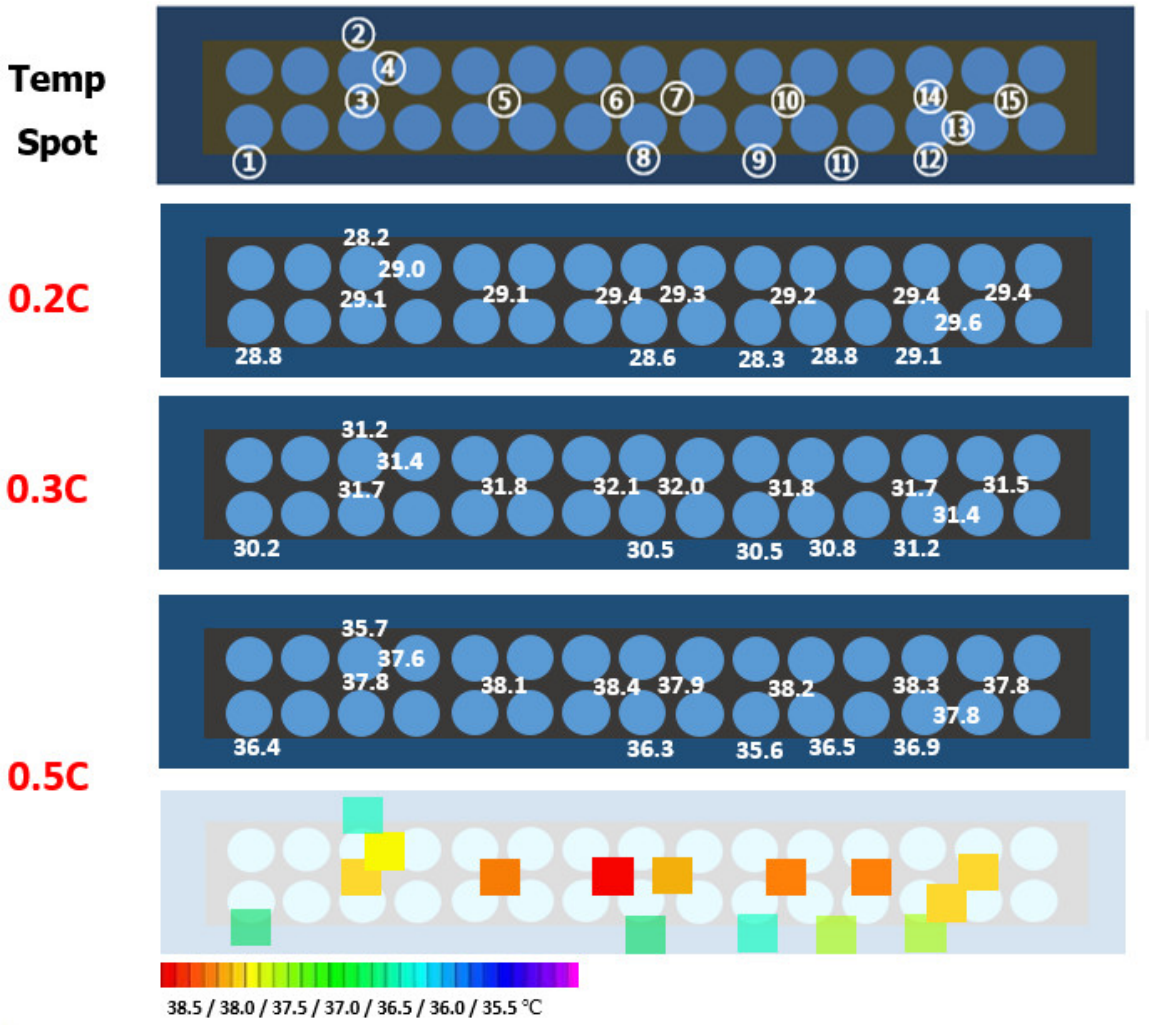

Figure S8. Temperature measuring spots and temperatures of BIF module during cycling

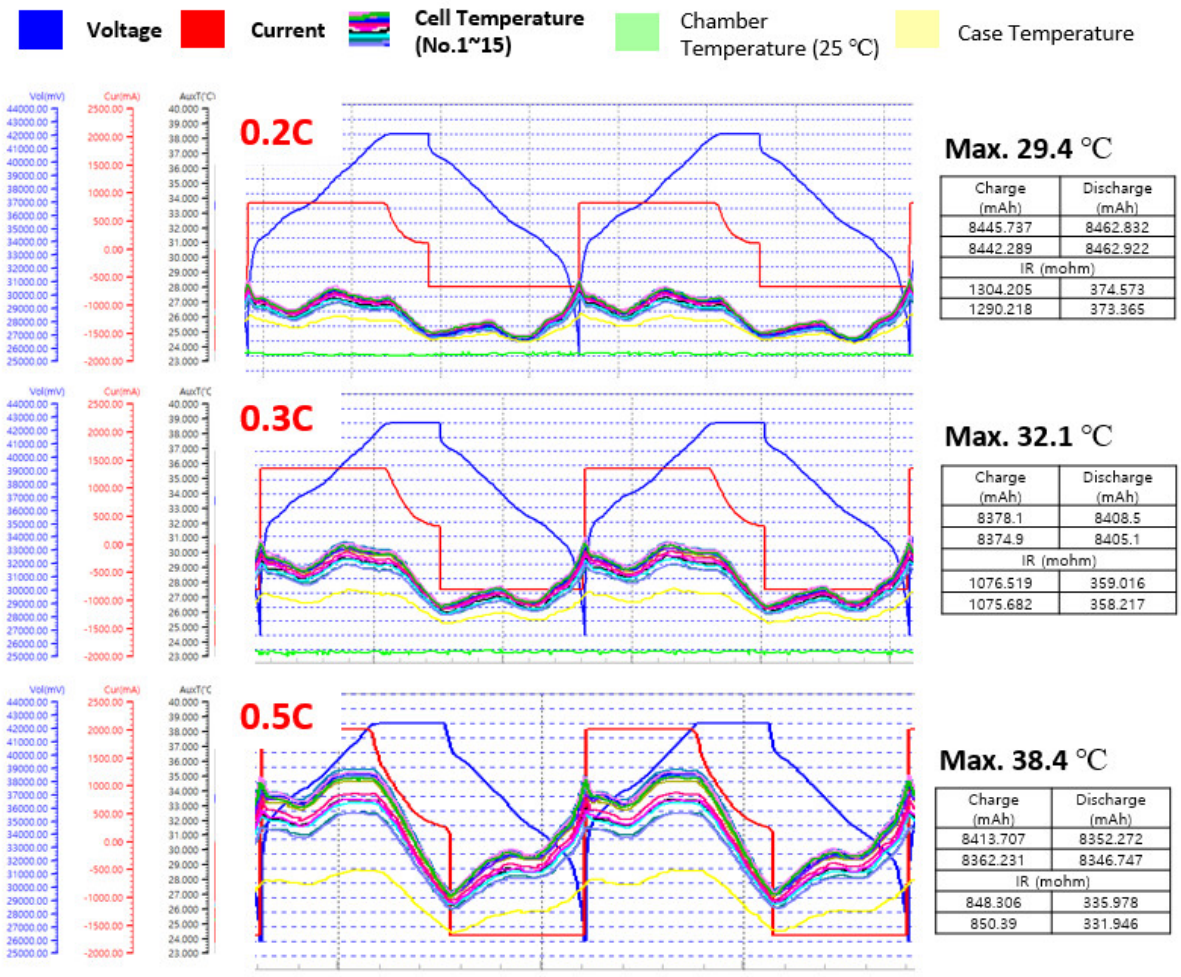

Figure S9. Electrochemical performances and temperatures of BIF module during cycling

Experimental – XCT of Protection Devices in Cylindrical Battery

There are generally approximately five protection devices in a cylindrical battery, namely, the CID, top vent, PTC, bottom vent, and protection circuit [18]. They are activated when the internal pressure exceeds standard conditions. The devices operated at high pressure, temperature, and current, known as PTC, are activated when the temperature exceeds 100 ºC. They have the advantages of being compact in size, lightweight, and easy to reset while having the disadvantages of increased cell resistance and energy density loss.

Figure S10 shows XCT data of cylindrical cells used in the BIF test before and after the operation under harsh conditions. Before cell cycling, the top disk and the PTC were separated, meaning that the anode and cathode of the battery were separated for normal operation. However, the cell reaching over 100 ºC activated the PTC operation, which led it to contact with the top disk.

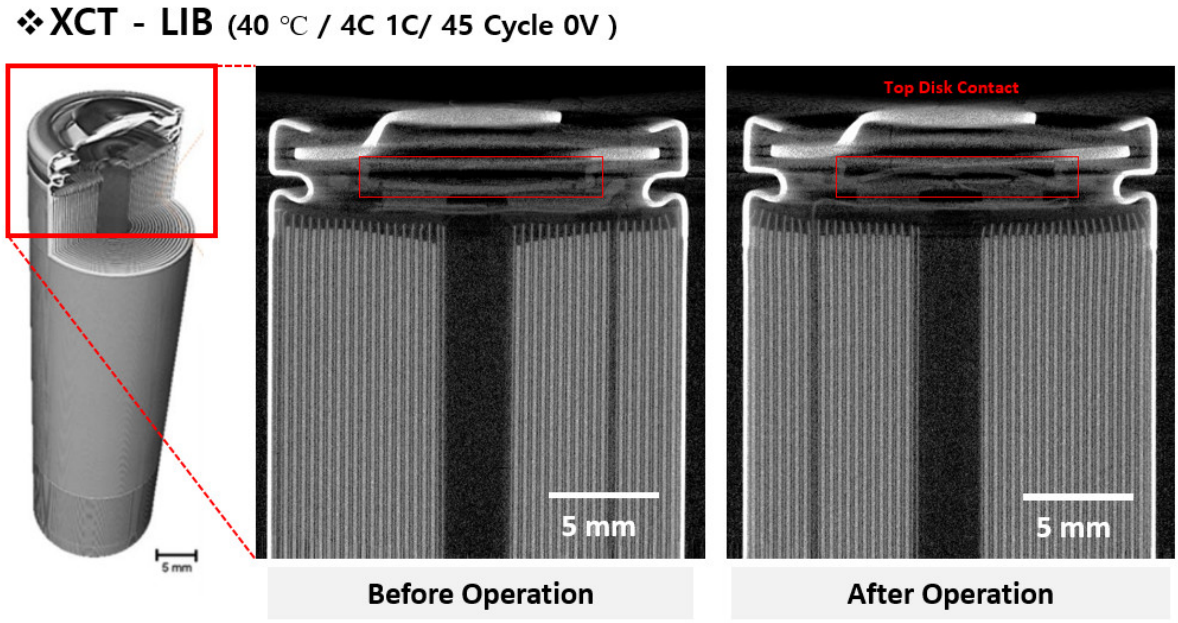

Figure S10. XCT data of the cylindrical cell before and after the operation